Available online at www.sciencedirect.com
SCIENCE DIRECT®
Journal of Crystal Growth 269 (2004) 41–49
JOURNAL OF CRYSTAL GROWTH
www.elsevier.com/locate/jcrysgro

Vacancy defects in epitaxial InN: identification and electrical properties

A. Laakso[a], J. Oila[a], A. Kemppinen[a], K. Saarinen[a,*], W. Egger[b], L. Liszkay[b,1], P. Sperr[b], H. Lu[c], W.J. Schaff[c]

[a] *Laboratory of Physics, Helsinki University of Technology, P.O. Box 1100, FIN-02015 HUT, Finland*
[b] *Institut für Nukleare Festkörperphysik, Universität der Bundeswehr München, D-85577 Neubiberg, Germany*
[c] *Department of Electrical and Computer Engineering, Cornell University, Ithaca, NY 14853, USA*

Abstract

We have used a low-energy positron beam to identify and quantify the dominant vacancy defects in InN layers grown on Al_2O_3 by molecular beam epitaxy. By applying both continuous and pulsed positron beams, we can show that In vacancies are formed during the crystal growth. Their concentration decreases from $\sim 5 \times 10^{18}$ to below 10^{16} cm^{-3} with increasing layer thickness (120–800 nm). The In vacancy concentration correlates with the free electron concentration and decreases with increasing electron Hall mobility. These results suggest that In vacancies act as both compensating defects and electron scattering centers in InN films.

PACS: 61.72.Hh; 78.70.B

Keywords: A1. Point defects; A1. Positron annihilation spectroscopy; A3. Molecular beam epitaxy; B1 InN

1. Introduction

The group III-nitride semiconductors GaN and AlN are interesting materials for applications in short-wavelength optoelectronic devices. Recent fascinating results suggest that indium nitride may have a bandgap of only 0.8 eV [1,2]. Hence, InN could extend the wavelength range of III-N materials into the infrared region. The high theoretical electron mobility and peak drift velocity also make InN a promising material for high-speed electronics [3,4]. The fabrication of device-quality InN has, however, been very difficult. One of the problems is related to the doping of InN. Due to donor states of unknown origin, the grown InN layers are highly n-type, and p-type doping has not been achieved. According to calculations, the impurities O_N and Si_{In} have the lowest formation energies of the donor-type defects [5], but also interstitial hydrogen is suggested to cause the n-type conductivity [6,7].

Another problem is the lack of a suitable substrate material. The large lattice mismatch with

*Corresponding author. Tel.: + 358-9-451-3111; fax: + 358-9-451-3116.
E-mail address: ksa@fyslab.hut.fi (K. Saarinen).
[1] On leave from KFKI Research Institute for Nuclear and Particle Physics, H-1525 Budapest P.O.B. 49, Hungary.

0022-0248/$ - see front matter © 2004 Elsevier B.V. All rights reserved.
doi:10.1016/j.jcrysgro.2004.05.032

the often-used Al_2O_3 substrate leads to a high density of extended defects. Among native defects, N and In vacancies are calculated to have the lowest formation energies, and are predicted to be relatively high when compared to native vacancies in for instance GaN [5]. Experimentally, the dominant point defects have not been identified and their concentrations are not known.

We have used positron annihilation spectroscopy [8] to study native vacancies in InN layers. Positrons get trapped at vacancies due to the missing positive ion core. The trapping can be experimentally observed through an increasing positron lifetime and as the narrowing of the momentum distribution of annihilating e^+e^- pairs. The positron lifetime is sensitive to the open volume of a defect (inverse electron density) and can thus be used to distinguish between mono- and di-vacancies, and larger vacancy clusters. The momentum distribution of the annihilating e^+e^- pairs can be measured as the Doppler broadening of the 511 keV annihilation radiation. This broadening reflects the momenta of the annihilating electrons, and it has chemical sensitivity that can be utilized to identify the atoms surrounding the vacancy defect.

In this work, we extend our previous study [9] by paying special attention to the positron lifetime data. In materials like InN, which do not exist in bulk form, the positron lifetime measurement can be performed by pulsing a low-energy beam [10]. This technique and the required apparatus has only recently been developed to the level required for defect studies [11]. On the other hand, positron lifetime spectra are required for a full understanding of results from positron annihilation spectroscopy, since only the lifetime experiment is able to distinguish unambiguously between positron annihilations in the lattice and those at vacancy defects.

Our results indicate the presence of a single type of vacancy in InN. By combining positron lifetime and Doppler broadening experiments, we can identify them as In vacancies or vacancy complexes containing V_{In}. The vacancy concentration correlates with free electron density and anticorrelates with the room temperature Hall mobility. This suggests that the vacancies are electron compensation and scattering centers, especially in the thinnest layers where the vacancy concentration is the highest.

2. Experimental details

The six InN layers studied were grown by molecular beam epitaxy (MBE) at Cornell University. The substrates were Al_2O_3 (0 0 0 1) with a 200 nm AlN buffer layer grown between the substrate and the InN layer. The thickness of the InN films varied between 120 and 800 nm (Table 1). On two films (the 120 and 380 nm films) a thin AlN cap was deposited on top of the InN layer. The films were not intentionally doped, but they had n-type conductivity with Hall carrier concentrations of 2×10^{18}–3×10^{19} cm^{-3}. The electron Hall mobility (300 K) is high, > 1100 $cm^2/V\,s$, in the thickest films, but decreases to below 200 $cm^2/V\,s$ in the thinnest layers. The results of the Hall measurements are single layer approximations of the non-uniform electron density and mobility.

The positron annihilation experiments were carried out using a variable energy positron-beam. The momentum distribution of the annihilating e^+e^- pairs was measured using the continuous positron beam at the Helsinki University of Technology. The Doppler broadening of the 511 keV annihilation line was recorded with a Ge-detector (resolution 1.3 keV at 511 keV). The low-momentum parameter S and the high-momentum parameter W were used to describe the

Table 1
The thickness, the free electron concentration and the electron (Hall) mobility for the studied InN layers. The In vacancy concentration was estimated from positron annihilation measurements

Sample no.	Thickness (nm)	n (sheet) (10^{14} cm^{-2})	μ (300 K) ($cm^2/V\,s$)	$[V_{In}]$ (cm^{-3})
1	120	3.8	175	$\geqslant 5 \times 10^{18}$
2	200	0.998	657	7×10^{16}
3	270	1.4	616	2×10^{17}
4	380	1.25	753	8×10^{16}
5	600	1.20	1165	$\leqslant 10^{16}$
6	800	1.7	1113	$\leqslant 10^{16}$

shape of the Doppler broadened line [8]. The probability of positron annihilation with low-momentum electrons increases when a positron is trapped at a vacancy, leading to an increase in the S parameter and a decrease in the W parameter.

The lifetime measurements were carried out using the pulsed positron lifetime beam facility at Universität der Bundeswehr in Munich [11]. With the pulsed positron beam the positron lifetime was measured as a time difference between the pulsing signal, corresponding to the time instant when the positron enters the sample, and the annihilation event detected by measuring the 511 keV radiation using a BaF_2 scintillation detector. The resolution was 290 ps and the peak-to-background ratio was better than 10^4. The lifetime spectra were analyzed carefully for each energy taking into account the uneven shape of the background and the resolution function, which was modelled as a sum of three Gaussians.

The pulsed beam enables the measurement of the positron lifetime distribution. The positron lifetime spectrum is a weighted sum of exponential decay components, $n(t) = \sum I_i \exp(-t/\tau_i)$, with lifetimes τ_i corresponding to the annihilations in different positron states, e.g. annihilation of a free positron in the InN lattice or annihilations of positrons trapped at vacancies. Experimentally, the positron trapping at vacancies is observed as an increase in the average positron lifetime $\tau_{ave} = \sum I_i \tau_i$.

3. Doppler broadening results

Fig. 1 shows the S parameter measured as a function of the positron beam energy (depth scan). At low positron incident energies ($E < 3$ keV) a fraction of the positrons are able to diffuse to the sample surface before annihilation. The high S parameter observed at low energies results from annihilations at the sample surface. In two of the samples (#1 and #4), the thin AlN cap on top of the InN layer is also visible in the curves. When the positron energy is increased, fewer positrons can reach the surface and the S parameter corresponds to annihilations inside the InN layer. The S parameter characteristic of the InN layer can be seen as a constant plateau in the curves. At higher implantation energies, the S parameter starts to decrease as positrons are able to reach the Al_2O_3 substrate below the InN. This turning point in the curves corresponds roughly to the layer thickness, except in sample #3 which seems to be thinner than expected from its nominal thickness (Table 1).

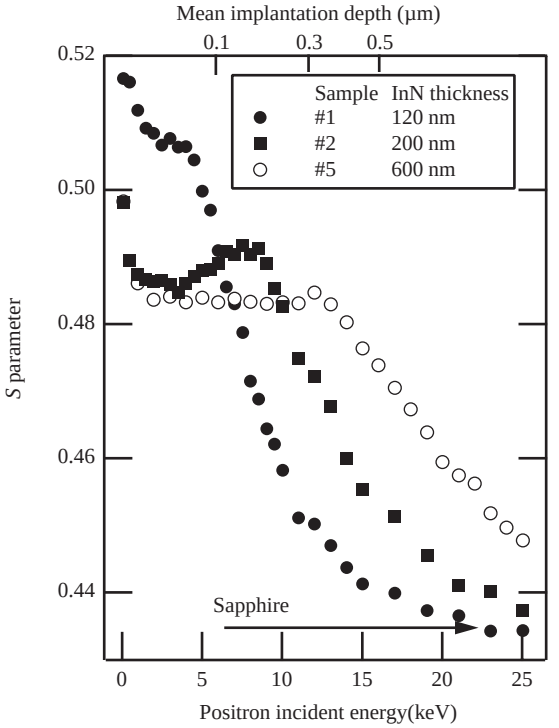

Fig. 1. The S parameter vs. positron beam energy for three different layers. The level associated with the sapphire substrate is shown with an arrow.

The lowest S parameter, $S \approx 0.483$ is found in the thickest (600- and 800-nm) layers (only #5 shown in Fig. 1). In the thinner layers the S parameter is clearly higher. The increased S parameter indicates that positrons get trapped at vacancy-type defects. In two of the samples (#2 and #3), the S parameter increases (and the W parameter decreases) towards the interface, suggesting that the vacancy concentrations are higher in the interface region.

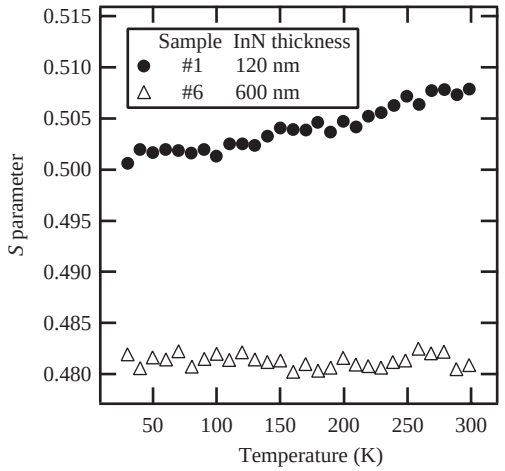

Fig. 2. The S parameter in two InN layers as a function of temperature. The positron beam energy was kept in the range $E = 3$–7 keV so that layer specific annihilation parameters were recorded.

The temperature dependence of positron annihilation parameters was studied between 30 and 300 K (Fig. 2). The positron beam energy was $E = 3$–7 keV, so that the layer-specific annihilation parameters would be recorded and so that the contributions from the surface and interfaces were minimized. In the thick layers (#5 and #6) the S and W parameters are constant as a function of temperature, which is typical for free positron annihilation in the lattice [8]. In the thin layers (e.g. #1 shown in Fig. 2) the S parameter is also almost constant, but shows a slight decrease with decreasing temperature. This kind of behavior is observed when positron trapping at a vacancy defect is in saturation and no annihilations take place in the lattice. The decrease of the S parameter may reflect the presence of negative ion defects, which compete with vacancies at low temperatures by trapping positrons at hydrogenic states with a low binding energy [8].

4. Positron lifetime results

The positron lifetime experiments, performed with the pulsed beam facility on four samples (#1, #3, #4, and #5) show very similar results compared to the Doppler measurements. The differences between samples are demonstrated in the lifetime spectra of Fig. 3. The 120 nm InN layer had clearly longer positron lifetime components than the 600 nm-thick sample, indicating vacancies in the thinner layer. The average positron lifetime τ_{ave} was 190 ps in the thickest layer (#5). In the thinnest layer, where the S parameter was also the highest, the average positron lifetime increased up to 260 ps.

The average positron lifetime τ_{ave} is plotted against implantation energy in Fig. 4. The lifetime distribution shows features similar to the S parameter in Fig. 1. The average lifetime in the layer decreases with increasing layer thickness. The significant increase in the average lifetime near the sample surface (low energies) is associated with positron diffusion to the surface where positrons get trapped by surface states with a long positron lifetime. The higher vacancy concentrations in the interface region can also be seen in the lifetime data of samples #4 and #5 as a slight increase in the average positron lifetime.

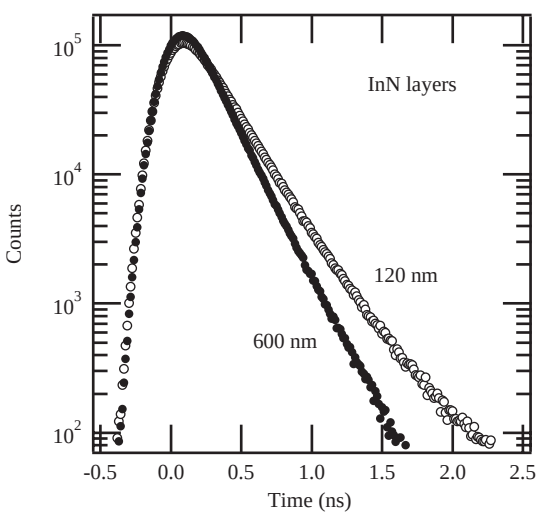

Fig. 3. Positron lifetime spectra from samples with 600 nm (black circles) and 120 nm layer (open circles) thicknesses. The spectra were measured with positron incident energies of 3 keV (120 nm layer) and 8 keV (600 nm layer). Positrons enter the sample at $t = 0$, and the vertical axis indicates the annihilation probability.

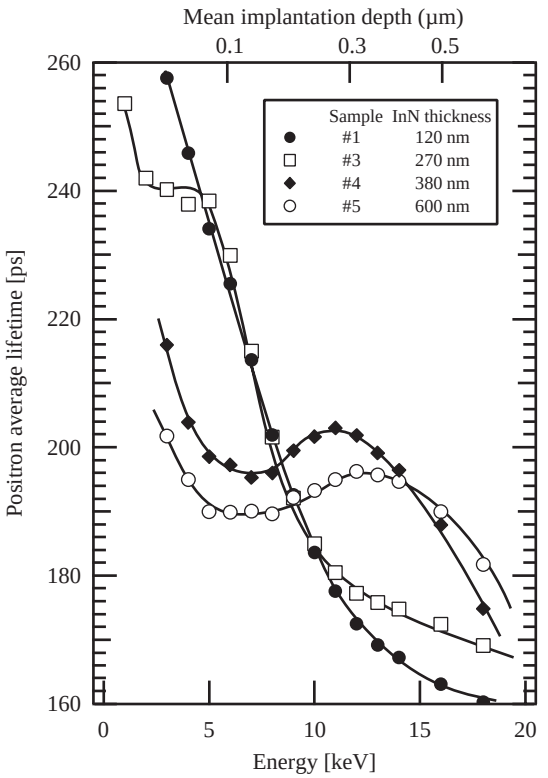

Fig. 4. The average positron lifetime τ_{ave} vs. positron beam energy (depth scan) for four different layers. The corresponding mean implantation depth of positrons is indicated on the top axis. The lines are a guide to the eye only.

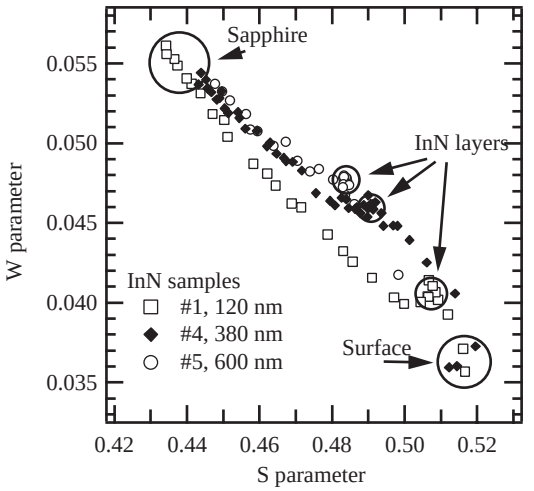

Fig. 5. W vs. S plot (positron beam energy as a running parameter) in three InN samples. The layer-specific parameters are clearly distinguished from the surface and sapphire substrate. The data points form a linear line between the sapphire and the InN layer, demonstrating no strong positron trapping effect at the interface.

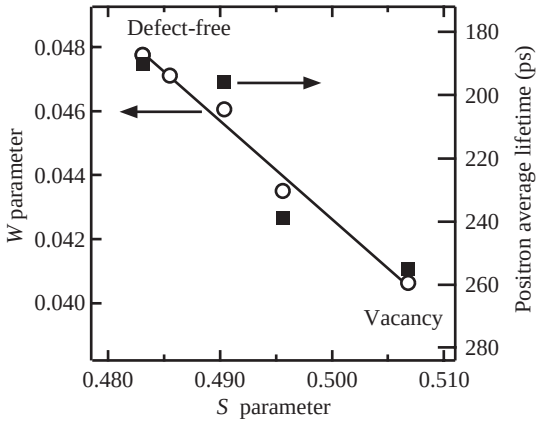

Fig. 6. The S and W parameters, and the average positron lifetime in the InN layers. The positron beam energy was kept in the range $E = 3$–7 keV so that the layer-specific annihilation parameters were recorded. The linearity between S and W, and between S and τ_{ave} indicates that the same vacancy is present in all layers.

5. Identification of In vacancy

5.1. Number of vacancy defect species by linearity analysis

The linearity between the annihilation parameters S,W and τ_{ave} can be utilized to investigate the number of different positron states in the samples [8]. The (S, W) plots, with positron energy as a running parameter, are shown in Fig. 5. When the positron energy is increased, the (S, W) points move from their surface values towards those specific for the InN layer, and finally towards the (S,W) point of the sapphire substrate. The data points form a straight line between the sapphire and the InN layer, indicating no strong contribution from the interfaces or from the buffer layer. The (S, W) parameters specific to each InN layer could thus be unambiguously determined.

Fig. 6 shows the layer-specific S and W parameters in each sample. The (S,W) points form a line, indicating that positrons annihilate in two states: as free positrons, characterized by the

annihilation parameters for defect-free InN (S_b, W_b), and as positrons trapped at a particular vacancy (S_V, W_V). Similarly, the functional relationship between the positron average lifetime and the S parameter is linear (Fig. 6), indicating again that the vacancy in each of the layers is the same [8].

5.2. Identification by chemical neighborhood and open volume

The identification of a vacancy defect can be based on both electron density (positron lifetime) and momentum density (Doppler spectroscopy) data. In Fig. 7, the high momentum part of the 511 keV annihilation line is shown for samples #1 and #6, measured with positron energies corresponding to the middle of the InN layer. The Doppler broadening spectra were recorded with a two-detector (Ge-BGO) coincidence set-up to reduce the background level [8]. In Fig. 7, the theoretical momentum distributions, which were calculated by using atomic core electron wave functions [12,13], are shown also for three different cases: the annihilations of free positrons in the defect-free InN lattice, and the annihilation of positrons trapped at In and N vacancies.

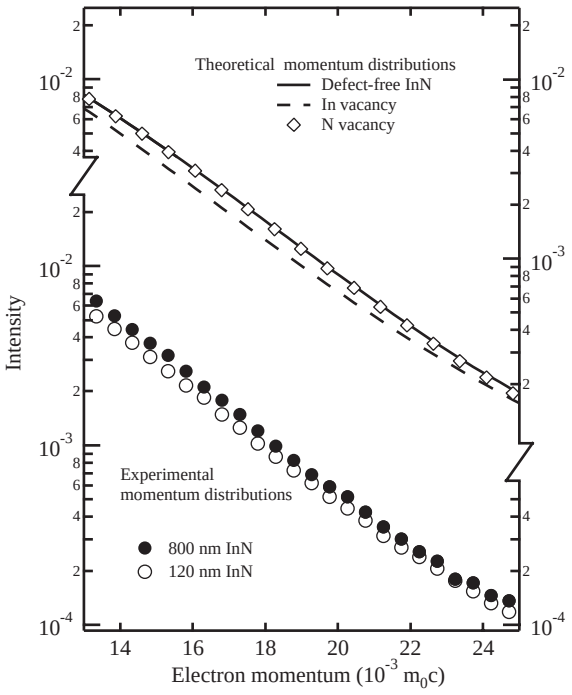

Fig. 7. The core electron momentum distributions in the InN layers. The lower panel presents the experimental results for samples #1 and #6, measured at beam energies of 2.5 and 7 keV, respectively. The upper panel shows the results of theoretical calculations for the InN lattice and for vacancies in both sublattices.

Above $15 \times 10^{-3} m_0 c$ the momentum distribution mainly consists of the annihilations with the atomic core electrons and therefore provides information on the atoms around the annihilation site. In the case of free-positron annihilation in defect-free InN, the strongest contribution to the high-momentum area comes from annihilations with the 4d-electrons of indium. For the N vacancy, the calculated wavefunction of positrons overlaps strongly with the neighboring In atoms, resulting in a momentum distribution very similar to that for free-positron annihilation. For the In vacancy, the strongest contribution also comes from the 4d-electrons of indium, but as the In atoms are now the second nearest neighbors, the intensity of the high momentum range is clearly smaller. The intensity reduction between the measured momentum distributions in the samples #6 (low vacancy concentration) and #1 (high vacancy concentration) indicates that the observed vacancies are In vacancies.

Further evidence is provided by the changes in the shape of the momentum distributions. As can be seen in Fig. 7, the slopes of the momentum distributions are slightly different for the vacancy (sample #1,120 nm) and lattice (sample #6, 800 nm). This small effect is due to N 2s and N 1s electrons, which have high momenta and enhance the intensity at (20–25) $\times 10^{-3} m_0 c$ in the curve obtained for the vacancy (sample #1, 120 nm). The vacancy is thus surrounded by N atoms, i.e. it is the In vacancy.

The identification of the In vacancy is supported also by the positron lifetime experiments. The positron lifetime in a defect-free InN lattice was calculated using the atomic superposition method [13,14] as 184 ps, and the lifetimes of positrons trapped at N and In vacancies were calculated as 186 and 260 ps, respectively. These are close to the

experimental average positron lifetimes of 190 ± 2 and 260 ± 2 ps in samples #1 and #5, respectively (Fig. 6). Although the decomposition of the measured lifetime spectra into free-positron and vacancy-related components is difficult, the observed difference of about 70 ps between the average positron lifetimes in the thin and thick samples (Fig. 6) can result only from positron trapping at In vacancies.

6. In vacancy concentrations

The positron lifetime spectrum measured in the thick layer (#5) consists mainly of one exponential decay component, indicating that almost all positrons annihilate as free positrons and that the vacancy concentration must be very low, below the detection limit of $\leqslant 10^{16}\,\mathrm{cm}^{-3}$. The Doppler broadening parameters S and W remain constant as the temperature is varied between 30 and 300 K (Fig. 2), which is typical for free positron annihilation in a lattice. We thus conclude that the annihilation parameters S_b, W_b, and τ_b recorded in the thickest layers represent those of vacancy-free InN.

In the standard positron trapping model, the vacancy concentration can be calculated from [8]

$$c_V = \frac{N_{at}}{\mu_V \tau_b} \frac{(S/S_b - 1)}{(S_V/S_b - S/S_b)}, \quad (1)$$

where S_V is the S parameter specific to the vacancy, μ_V the positron trapping coefficient, $N_{at} = 6.367 \times 10^{22}\,\mathrm{cm}^{-3}$ is the atomic density, and τ_b the positron lifetime in vacancy free InN. Typically, the vacancy-specific S parameter for the monovacancy [8] is about $1.03\text{–}1.05 \times S_b$ (e.g. $S_V \approx 1.046 \times S_b$ for V_{Ga} in GaN [14]). The S parameter in the thinnest layer (#1) is about 4.9% higher than in the thickest layers. The average lifetime in the thinnest layer is also much higher, the difference in lifetimes being about the same as the calculated difference for the V_{In}. Together these suggest that in the thinnest layer (#1) all positrons get trapped at vacancies and evidently the concentration of the vacancies is very high. A determination of the exact vacancy concentration is therefore not possible, but a lower limit estimate for the concentration is about $5 \times 10^{18}\,\mathrm{cm}^{-3}$.

The vacancy concentration in other samples (Table 1) were estimated by using $\tau_b = 184$ ps and the S parameters recorded in the thickest and thinnest layers as S_b and S_V, respectively. We further take $\mu_V = 2 \times 10^{15}\,\mathrm{s}^{-1}$, which is a typical value for negative vacancies [8]. As a result, the In vacancy concentration decreases more than two orders of magnitude when the layer thickness increases from 120 nm to above 600 nm (Table 1).

The vacancy concentrations in Table 1 correspond to the middle of the InN layer, weighted with the positron stopping profile. Since the standard deviation of the positron distribution is typically half of the layer thickness [8], the depth resolution of the measurement is poor and the highly defected region close to the interface is not observed in the thickest layers. Since the growth is reproducible and the thinner films represent the earlier stages of growth in thicker films, the V_{In} concentrations in Table 1 can be taken as a depth profile which shows that the In vacancy concentration increases towards the interface. In fact, the higher vacancy concentration closer to the InN/Al_2O_3 interface is also seen directly in the S and W vs. E and τ_{ave} vs. E curves in Figs. 1 and 4.

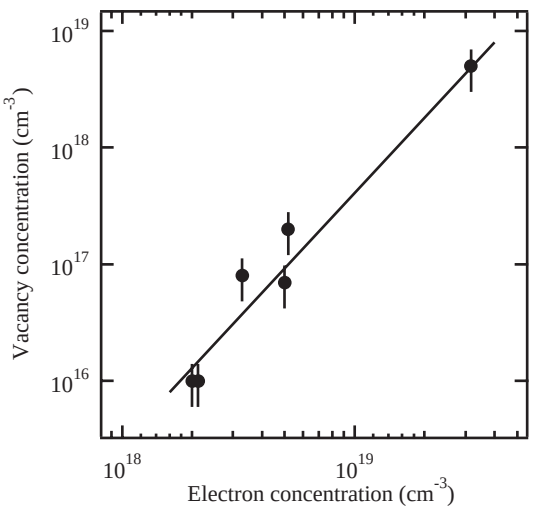

Fig. 8. In vacancy concentration vs. electron concentration. vacancy concentration is found to correlate with free electron density, as expected for compensating centers in n-type InN.

The In vacancy concentration is presented in Fig. 8 as a function of the free electron density, obtained by dividing the measured sheet carrier concentration by the thickness of the layer. The concentration of V_{In} increases by about three orders of magnitude with the free electron density. This behavior is typical for compensating acceptor defects in highly n-type material. Furthermore, the results show that n-type doping concentrations of more than $10^{18}\,cm^{-3}$ can be reached without significant compensation due to In vacancies. This is similar as recently observed for the MBE growth of GaN [15].

According to theory [5], the In vacancy has the lowest formation energy of all neutral and negatively charged defects, when the Fermi level is close to the conduction band. This is in agreement with our results in respect to the observation of In vacancies. On the other hand, the formation energy of V_{In} is predicted to be high [5], suggesting that their concentration should be much lower than determined here. The high vacancy concentration closer to the InN/Al_2O_3 interface suggests that the formation of the vacancies could be related to the presence of other defects, e.g. dislocations or impurities, and to strain at the interface region. The presence of In vacancies could also reflect the N rich stoichiometry of the material, as determined by elastic recoil detection analysis [16]. The N vacancy, which has a low formation energy according to theory [5], could also be present but escapes detection by positrons due to the positive charge state.

The quality of InN has been shown to increase with increasing layer thickness [17,18]. This is evident also in the samples of this study, where the room temperature Hall mobility increases from below 200 to above $1100\,cm^2/V\,s$ as the layer thickness is increased (Fig. 9). The enhanced electron mobility indicates that the defect densities are reduced at greater distances from the interface. The vacancy concentration simultaneously undergoes a drastic decrease (Fig. 9), suggesting that the observed vacancies limit the electron mobility even at room temperature by acting as scattering centers.

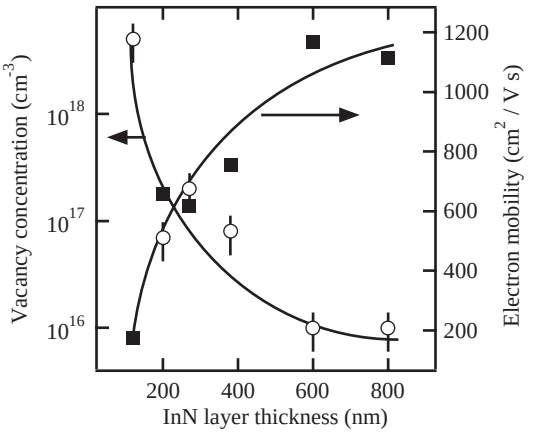

Fig. 9. Electron Hall mobility and In vacancy concentration as a function of the InN layer thickness.

7. Conclusions

In summary, we have observed vacancies in MBE-grown InN layers with positron annihilation spectroscopy, using both positron lifetime and Doppler broadening measurements. The concentration of vacancies decreases with increasing layer thickness. The defects are identified as In vacancies. The increase in $[V_{In}]$ from below 10^{16} to above $10^{18}\,cm^{-3}$ for films of increasing thickness correlates with the increase of the free electron density. This behavior is typical for a compensating center. The concentration of In vacancies also anticorrelates with the electron Hall mobility, suggesting that the $[V_{In}]$ may significantly limit electron mobility in the thinner layers.

Acknowledgements

The work has been partly financed by the Academy of Finland (DENOS project). The authors also acknowledge the support of Colin Wood at the Office of Naval Research.

References

[1] V.Yu. Davydov, A.A. Klochikhin, R.P. Seisyan, V.V. Emtsev, S.V. Ivanov, F. Bechstedt, J. Furthmüller, H.

Harima, A.V. Mudryi, J. Aderhold, O. Semchinova, J. Graul, Phys. Stat. Sol. b 229 (2002) R1.
[2] J. Wu, W. Walukiewicz, K.M. Yu, J.W. Ager III, E.E. Haller, H. Lu, W.J. Schaff, Y. Saito, Y. Nanishi, Appl. Phys. Lett. 80 (2002) 3967.
[3] E.B. Bellotti, B.K. Doshi, K.F. Brennan, J.D. Albrecht, P.P. Ruden, J. Appl. Phys. 85 (1999) 916.
[4] B.E. Foutz, S.K. Leary, M.S. Shur, L.F. Eastman, J. Appl. Phys. 85 (1999) 7727.
[5] C. Stampfl, C.G. Van de Walle, D. Vogel, P. Krüger, J. Pollmann, Phys. Rev. B 61 (2000) R7846.
[6] D.C. Look, H. Lu, W.J. Schaff, J. Jasinski, Z. Liliental-Weber, Appl. Phys. Lett. 80 (2002) 258.
[7] E.A. Davis, S.F.J. Cox, R.L. Lichti, C.G. Van de Walle, Appl. Phys. Lett. 82 (2003) 592.
[8] K. Saarinen, P. Hautojärvi, C. Corbel, In: M. Stavola (Ed.), Identification of Defects in Semiconductors, Academic Press, New York, 1998, p. 209.
[9] J. Oila, A. Kemppinen, A. Laakso, K. Saarinen, W. Egger, L. Liszkay, P. Sperr, H. Lu, W.J. Schaff, Appl. Phys. Lett. 84 (2004) 1486.
[10] A. Laakso, K. Saarinen, P. Hautojärvi, Physica B 308–310 (2001) 1157.
[11] W. Bauer-Kugelmann, P. Sperr, G. Kögel, W. Triftshäuser, Mater. Sci. Forum. 363–365 (2001) 529.
[12] M. Alatalo, H. Kauppinen, K. Saarinen, M.J. Puska, J. Mäkinen, P.Hautojärvi, R.M. Nieminen, Phys. Rev. B 51 (1995) 4176.
[13] M. Alatalo, B. Barbiellini, M. Hakala, H. Kauppinen, T. Korhonen, M.J. Puska, K. Saarinen, P.Hautojärvi, R.M. Nieminen, Phys. Rev. B 54 (1996) 2397.
[14] K. Saarinen, P. Seppälä, J. Oila, P. Hautojärvi, C. Corbel, O. Briot, R.L. Aulombard, Appl. Phys. Lett. 73 (1998) 3253.
[15] M. Rummukainen, J. Oila, A. Laakso, K. Saarinen, A.J. Ptak, T.H. Myers, Appl. Phys. Lett. 84 (2004) 4887.
[16] H. Timmers, S.K. Shrestha, J. Crystal Growth, these proceedings doi:10.1016/j.jcrysgro.2004.05.033
[17] S. Yamaguchi, M. Kariya, S. Nitta, T. Takeuchi, C. Wetzel, H. Amano, I. Akasaki, J. Appl. Phys. 85 (1999) 7682.
[18] H. Lu, W.J. Schaff, J. Hwang, H. Wu, G. Koley, L.F. Eastman, Appl. Phys. Lett. 79 (2001) 1489.